

Hindered stokesian settling of discs and rods

Yating Zhang and Narayanan Menon
*Department of Physics, University of Massachusetts,
Amherst, Massachusetts 01003, USA*

(Dated: November 22, 2024)

We report measurements of the mean settling velocities for suspensions of discs and rods in the stokes regime for a number of particle aspect ratios. All these shapes display "hindered settling", namely, a decrease in settling speed as the solid volume fraction is increased. A comparison of our data to spheres reveals that discs and rods show less hindering than spheres at the same relative interparticle distance. The data for all six of our particle shapes may be scaled to collapse on that of spheres, with a scaling factor that depends only on the volume of the particle relative to a sphere. Despite the orientational degrees of freedom available with nonspherical particles, it thus appears that the dominant contribution to the hindered settling emerges from terms that are simply proportional to the volume of the sedimenting particles.

Sedimentation, the gravitational settling of solid particles in a liquid, presents a complex challenge in classical many-body physics, particularly in the highly-viscous, overdamped Stokes regime where particle velocity fields decay very slowly with distance r from the particle, as $1/r$. Many puzzles have emerged in studies of the sedimentation of suspensions of spheres[1–5], especially on the scaling of fluctuations with system size. In this article we address a basic question on the mean sedimentation rate in the collective settling of suspensions of *non-spherical* particles, which are far more common in natural and technological sediments such as clays, snowflakes, ice crystal, minerals, phytoplankton, reaction precipitates or paper fibres.

The question we wish to address is how the settling velocity V_S of an isolated particle of typical size ℓ in a fluid of viscosity η and density ρ is modified by the presence of a finite volume fraction ϕ of other particles. Our focus is on the Stokes regime where the Reynolds number $Re = \rho V_S \ell / \eta \ll 1$. This effect is captured by the "hindered settling function" $H(\phi)$, a dimensionless ratio defined as $H = V/V_S$, where $V = V(\phi)$ is the mean sedimentation velocity of particles in suspension and V_S is the stokes velocity of an isolated particle. As the name implies, in suspensions of spheres, settling is hindered, with a monotonic decrease from $H(0) = 1$ as volume fraction ϕ is increased[6, 7]. Brzinski and Durian[8] made an extensive compilation of data for sphere-sedimentation from previous studies. These studies include data for both small Pe (brownian) and large Pe (non-brownian), where the Péclet number $Pe = V_S \ell / D$ with diffusion coefficient D , quantifies the relative efficacy of convective to diffusive transport. These data are typically fit by the empirical Richardson-Zaki form $H(\phi) = (1 - \phi)^n$ [9] with best-fit values of $n \approx 4.5$ for the large Pe , non-brownian regime that we consider in this article. There is no theory of $H(\phi)$ over the entire range of volume fractions; indeed, the only rigorous hydrodynamic calculation owes to Batchelor[10] who predicted that in the dilute limit, $\phi \rightarrow 0$, $H(\phi) = 1 - 6.55\phi + \mathcal{O}(\phi^2)$.

Shape leads to a qualitative difference in single particle

dynamics and pair interactions: while a single sphere falls straight down without rotation, rods, discs, and ellipsoids drift horizontally and have vertical settling speeds that depend on their orientation relative to gravity[11–15]. A pair of spheres falls faster than one sphere, remaining at fixed separation[16], however pairs of discs settling at low Reynolds number display either bound periodic orbits or scattering states[17, 18] due to the coupling between orientational and translational degrees of freedom. Likewise, a sedimenting lattice of disc shows very different collective behaviour[19] than a lattice of spheres[20].

However, the central question of this article is whether the effects of orientational degrees of freedom lead to a significant difference in collective behaviour of a finite volume fraction – as opposed to a finite number – of shaped particles compared to sphere suspensions, where many more studies exist. A prominent example of previous work is the sedimentation of rod-like particles studied in a series of papers by Guazzelli and coworkers[21–25], who identified two distinct regimes of sedimentation for fibers: at higher volume fractions, they observe hindered settling reminiscent of sphere-suspensions, whereas at low enough volume fractions where the fibres can rotate freely without steric hindrance, sedimentation leads to a complex pattern of instabilities. We are not aware of comparable studies for the geophysically relevant case of flat particles at finite volume fraction.

In this article, we present new data on the hindered settling of flat shapes (discs and hexagons) and elongated shapes (rods) in the Stokes regime, as a function of both particle aspect ratio and solid volume fraction, while remaining in a semi-dilute regime, as discussed later. These shapes are nonpolar (i.e. head-tail symmetric) and effectively axisymmetric. Despite the wide range of aspect ratio of particles that we explored, our principal observation is that the dominant contribution to the hindered function $H(\phi)$ emerges from terms proportional to the volume of a single particle.

We report results for three different aspect ratios each of flat (discs, hexagons) and long shapes (rods). All particle dimensions are given in Table I with the radius c ,

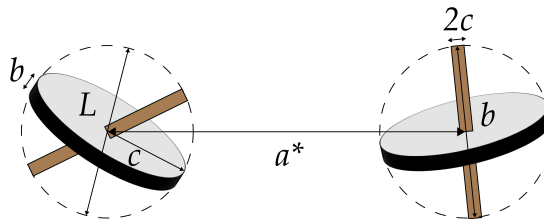


FIG. 1: Data for discs and rods are compared to those of spheres held at the same normalized separation $a^* = a/L$, where a is the mean interparticle separation and L is the largest particle dimension, i.e. diameter $2c$ of hex and discs or the length b of rods.

TABLE I: Particle geometry, measured Stokes velocity, Reynolds number and Péclet number

Aspect ratio, shape	c (mm)	b (mm)	V_S (mm/s)	Re	Pe
A=0.15 hex	0.27 ± 0.01	0.08 ± 0.001	0.04 ± 0.001	6.33×10^{-5}	1.07×10^{10}
A=0.07 hex	0.65 ± 0.02	0.09 ± 0.003	0.13 ± 0.003	4.96×10^{-4}	1.36×10^{11}
A=0.05 disc	0.66 ± 0.003	0.06 ± 0.002	0.10 ± 0.004	3.88×10^{-4}	1.32×10^{11}
A=19 rod	0.15 ± 0.0003	5.69 ± 0.012	0.36 ± 0.004	4.25×10^{-4}	6.65×10^{12}
A=10 rod	0.26 ± 0.0009	5.45 ± 0.030	0.42 ± 0.004	2.37×10^{-4}	2.07×10^{13}
A=3 rod	0.49 ± 0.0004	2.97 ± 0.015	0.89 ± 0.001	2.74×10^{-4}	4.34×10^{13}

thickness/length b , and aspect ratio $A = b/2c$. The error bars, measured by the standard error on a small population of individual particles, shows that the discs, hex, and especially the rods, are very monodisperse. The rods were stainless steel, and used after cleaning and demagnetization in a degaussing coil. The discs and hex particles were polyimide, and used as purchased.

The particles are suspended in silicone oil of three different viscosities, $\eta = 350, 5000$ or 10000 cSt , chosen to produce a Reynolds number Re of approximately 10^{-5} to 10^{-4} in all situations. To obtain a known volume fraction ϕ , we first measured the density of the solid particles using a pycnometer (EISCO Labs). We first filled the pycnometer of $10 \pm 0.03ml$ with distilled water to ascertain its precise volume. We then added a known mass of particles and a few drops of 1% soap solution which suppressed bubbles from adhering to solid surfaces, then filled the container with distilled water. Using the measured density of the fluid, we were able to calculate the density of the particles. The precise volume of the sedimentation cell is then measured, and a sample of known volume fraction ϕ can be prepared with a precision of $\pm 3\%$.

We placed partially filled sample containers and a beaker of silicone oil in a vacuum chamber for more than 24 hours to remove bubbles. The sample containers were then nearly fully filled with silicone oil from the beaker. We applied vacuum again for several hours to remove the remaining bubbles and then overfilled the samples with silicone oil. Next, we sealed the bottles with Teflon tape and threaded lids. Once a sample was prepared, we put them in a home-built tube rotator for mixing overnight at low frequency (a few r.p.m.) to generate a well-mixed homogeneous state at the chosen volume fraction ϕ .

The specimens are then quickly placed vertically with

a precision of $\pm 0.2^\circ$. The settling process was observed by taking images with a Nikon DSLR camera of the entire cell at fixed time intervals of typically $5s$ until all solid particles have settled at the bottom. For white particles (the hex and discs) we illuminated the sample from the side and observed light scattered by particles into the camera, whereas for the opaque rods, we chose back lighting to produce a high contrast, as shown in Fig. 2(a)&(b).

To obtain $V(\phi)$, the sedimentation velocity, we adopted a method based on that of Ref. [8]. As shown in Fig. 2(a)&(b), we select a central rectangular region, and identify the position of the interface by taking gradients of the smoothed, horizontally-averaged intensity profile shown in Fig. 2(c). To show the outcome of this process, we display in Fig. 2(d) a time-series of eighteen images stitched together. The upper green dots are the identified location of the interfaces between the suspension and the supernatant fluid. The upper red line is a fit to the green dots that represent the top interface. This is well-fit by a straight line, implying that the sedimentation velocity $V(\phi)$ is constant over the entire settling process, and that the mean sedimentation is a steady state process. This in turn implies that the sample was well mixed initially and reproducibly prepared.

In a few cases, it is hard to detect the interface of suspension and the supernatant fluid when scattering or absorption of the illumination by the particle does not form a sharply-defined interface. Here we used the OpenPIV package for Particle Image Velocimetry to detect the velocity of individual particles and averaged over many particles to obtain the sedimentation velocity V .

In addition to the velocity $V(\phi)$ with which the top interface recedes, for the flat particles which we image by scattered light, we also obtain the velocity V_p with which the solid precipitate front grows, as shown by the lower

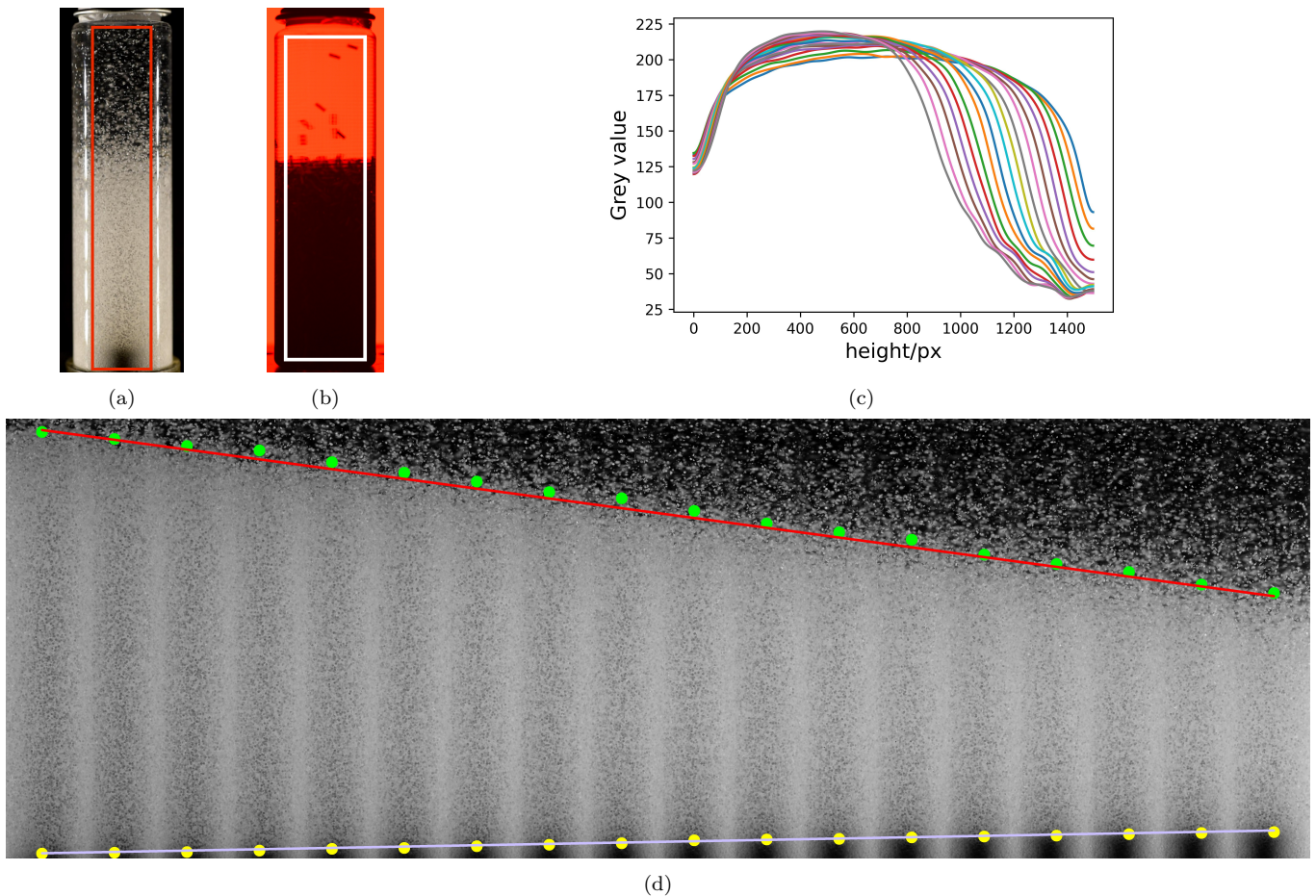


FIG. 2: (a) Sample of $\phi = 0.04$, $A = 0.15$ hex particles imaged with scattered light. (b) Sample of $\phi = 0.18$, $A = 3$ rods imaged with transmitted light. The rectangles show the region selected for analysis. (c) Grey value of all selected images from (a), as a function of height at a series of times. The grey value is the intensity averaged over the horizontal direction. (d) Image sequence for the sample in (a). The dots are the center points of interfaces found by analyzing the gradient of curves in (c). Green dots mark the interface detected between the suspension and the supernatant fluid. The yellow dots mark the interface between the suspension and the sediment solid. The red and purple lines are fits to the two sets of interface positions, whose slopes represent the sedimentation velocity V and the velocity V_p of the advancing solid precipitate, respectively.

set of yellow symbols and the purple line in Fig. 2(d). Mass conservation of the solid implies $V\phi + V_p(\phi - \phi_p) = 0$, which allows us to extract the volume fraction ϕ_p of the precipitate[29]. All the sedimentation velocity data are tabulated in the Supplemental Material[29].

To obtain the hindered function $H(\phi)$ from V , we normalize by the stokes velocity V_S . We determined the stokes velocity from measurements of a single particle dropped in a container much larger than the particle size. A complication is that V_S for an anisotropic particle depends on orientation. We measured V_S for vertically oriented rods, but the hex and discs were too small to fix an initial orientation, and the data averages over initial orientations. All the data are shown in Table I.

Finite size effects arising from the wall are expected to be smaller for the sedimentation velocity V itself, due to screening of the wall effect in the bulk. We confirm

this expectation for a series of $\phi = 0.04$, $A = 0.15$ hex samples in containers with varying heights and widths as shown in the Supplemental Material[29].

In Fig. 3(a) we show the principal experimental results of this article. Rather than as a function of ϕ , we plot the hindered settling function as a function of $a^* = a/L$, namely, the interparticle separation, a , normalized by the largest dimension L of the particle i.e. the diameter of hex and discs, and length of rods (see Fig. 1). The interparticle separation, a is computed from the experimental volume fraction ϕ assuming a random spatial distribution of particles[30, 31]. That is, $a^* = a/L = k\phi^{-1/3}$, where $k = 0.447$ for spheres, and k depends on aspect ratio A for rods and discs as specified in the Supplemental Material[29].

The data shown in Fig. 3(a) indicate a monotonically increasing trend for $H(a^*)$, showing that the effect of

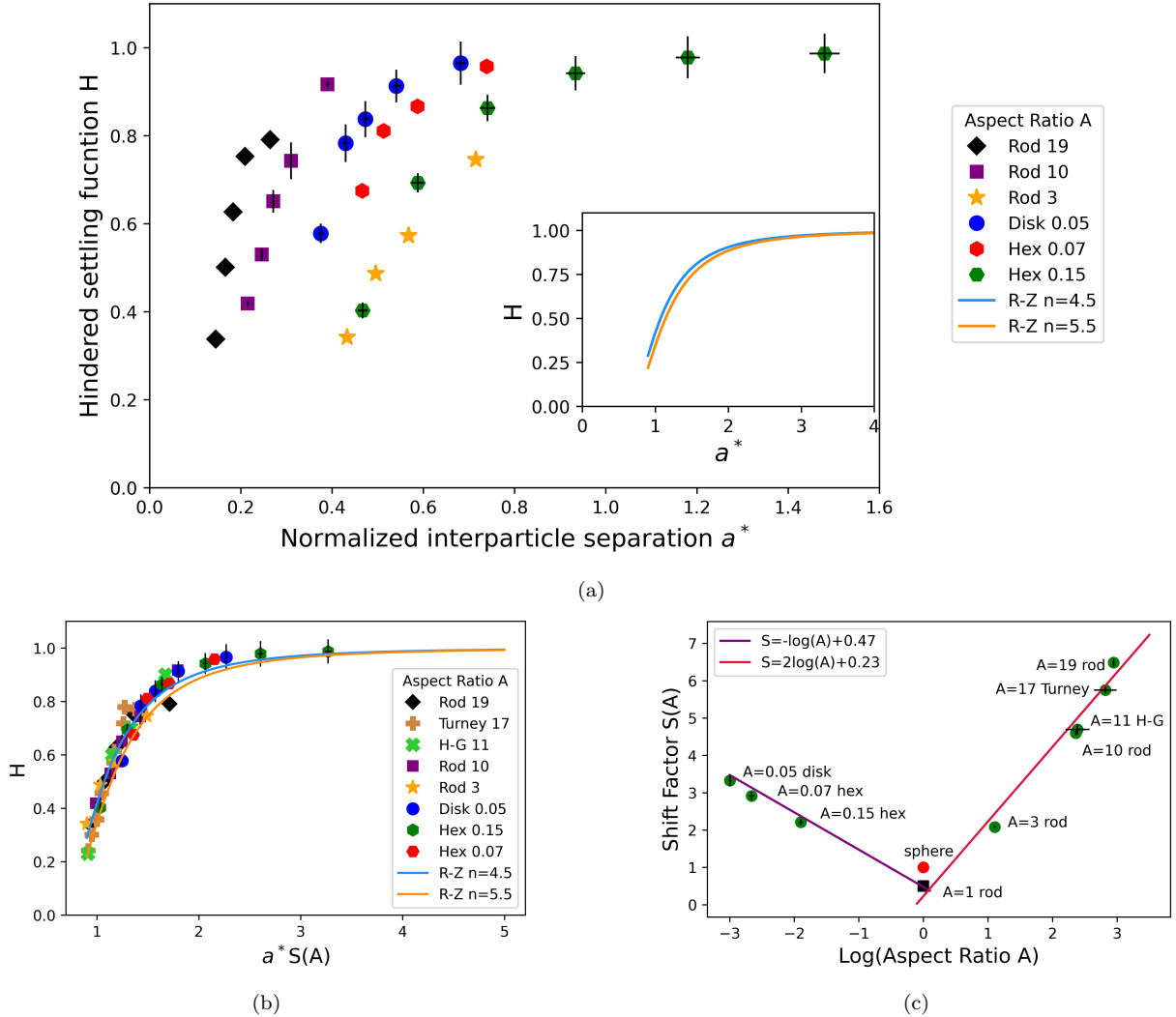


FIG. 3: (a) Hindered settling function H increases as normalized interparticle separation a^* increases for all particles we measured. Inset: The blue and orange curves are the Richardson-Zaki form $H = (1 - 0.18(a^*)^{-3})^n$, with $n=4.5$ & 5.5 respectively[9], which represent fits to sphere sedimentation. (b) $H(a^*)$ data shifted by a factor $S(A)$ to collapse on the R-Z curve with $n = 4.5$ based on the total least square method[26, 27]. We also include data from Herzhaft & Guazzelli and Turney *et al.* [22, 28]. (c) Shift factor $S(A)$ versus the logarithm of the aspect ratio A for both flat and long particles. The red dot for spheres is by definition at $S = 1$, $A = 1$. We also show a black square to indicate a cylinder with $A = 1$, placed at the appropriate volume relative to the sphere.

increasing volume fraction is indeed to hinder collective sedimentation, as is the case with spheres. As a point of reference, we show in the inset curves for the Richardson-Zaki function with $n = 4.5$ and 5.5 (which represent global fits[8] to data for spheres at $Pe > 10^8$ and $Pe < 10^8$, respectively, in this regime of volume fraction). By comparison, deviations from $H = 1$ appear at smaller interparticle separation $a^* < 1$, or $a < L$, in a regime where the particles cannot rotate freely. Said differently, with the same relative spatial distribution, non-spherical particles show much less hindering than spheres indicating

that spheres occupy a significantly higher hydrodynamic volume than nonspherical particles.

To more quantitatively compare between different aspect ratio, A , we shifted the data for each shape by a factor $S(A)$ to achieve the best possible collapse against spheres, by minimizing the total least squared[26, 27] deviation between the data and the Richardson-Zaki function with $n = 4.5$, as shown in Fig. 3(b). We also included data from Herzhaft & Guazzelli and Turney *et al.* [22, 28] in Fig. 3(b), shifted in the same manner. To the extent that these eight data sets collapse within experimental error, the shift factor $S(A)$ captures the shape-dependence of the hindering effect of equally spaced particles with

equal largest dimension.

To explore further this shape dependence, we plot in Fig. 3(c) the shift factor $S(A)$ against the logarithm of the aspect ratio A . $S(A)$ for $A < 1$ (flat shapes) and $A > 1$ (rods) proportional to A^{-1} and A^2 respectively, with prefactors of order unity. When scaled to the largest particle dimension L , these aspect ratio dependencies capture the relative volume of these shapes, with the volume of sphere, disc and rod expressed as $\pi/6, \pi A/4$ and $\pi/(4A^2)$ in units of L^3 . Thus the scaling of the shift factor $S(A)$ as A^{-1} for discs and A^2 for rods is exactly the ratio of volume of the sphere to the volume of the shape. We note that the point for spheres, set at $S(A) = 1, A = 1$, lies above the intersection of the rod and the disc scaling. This is to be expected, as the volume of the inscribed sphere is less than the volume of the cylinder with $A = 1$ that should lie at the intersection point.

The data thus point to the significance of particle volume in hindering. We return to discuss the dominant contributors to hindering first. As mentioned earlier, for spheres in the dilute limit ($\phi \rightarrow 0$), Batchelor found $H(\phi) = 1 - 6.55\phi + \mathcal{O}(\phi^2)$ [10]. In this calculation, the dominant contribution to the hindering is from backflow. When particles settle, they must displace fluid upwards equal to their volume. In addition, a settling particle also drags the surrounding fluid down, which scales with the sphere volume. This is irrelevant for a single particle as the return flow is at infinity, but for a finite volume fraction, the corresponding volume of upward backflow goes through the bulk of the suspension. These two contributions amount to -5.5ϕ out of the -6.55ϕ . Only the remainder comes from hydrodynamics interactions that go beyond the mean flow: -1.55ϕ and $+0.5\phi$ come from the probability of close encounters among spheres and the hydrodynamic interactions via the second derivative of the velocity field generated by other spheres[1, 10]. We

are not aware of detailed calculations beyond the dilute regime for the relative contributions of backflow (both from the solid and the entrained fluid) versus interparticle hydrodynamic interactions. For the same relative spatial distribution and number density, ϕ is determined by the solid volume of individual particles. Then the backflow which dominates the hindering is proportional to the volume of the particle. This explains why the shift factor $S(A)$ for discs and rods is captured by the ratio of their solid volume to that of a sphere.

Our data therefore suggest that the mean hindered settling of discs and rods in the stokes regime are to a first degree not more complicated than that of spheres, despite the orientational degrees of freedom that potentially add new physics to the sedimentation of shaped particles. Subtler effects such as the width of the sedimentation interface or fluctuations that could be introduced by the orientational degrees of freedom remain to be explored in systems of shaped particles.

We also note that our conclusions are formed based on experiments in the semi-dilute regime where interparticle separation is of the order of the particle size. At lower volume fractions, rods, at least, have been shown to experience segregation into dense lanes of streamers and particle-depleted regions where the backflow can bypass particle-rich regions. These instabilities appear to be system-size dependent and the boundary between the stable, hindered, region and the unstable regions deserves further exploration. Of course, as one enters higher density regimes, translational and orientational degrees of freedom can become constrained due to both steric and hydrodynamic interactions and then more complicated physics can emerge.

We gratefully acknowledge financial support through NSF-DMR 2319881. We thank D.J. Durian and V. Mathai for their help with the literature, and A. Rodrigues for her help with density measurements on discs.

-
- [1] P. Chaikin, Thermodynamics and hydrodynamics of hard spheres: the role of gravity, *Soft and Fragile Matter, Nonequilibrium Dynamics, Metastability and Flow*, 315 (2000).
- [2] R. E. Caflisch and J. H. Luke, Variance in the sedimentation speed of a suspension, *Physics of Fluids* **28**, 759 (1985).
- [3] H. Nicolai, B. Herzhaft, E. Hinch, L. Oger, and E. Guazzelli, Particle velocity fluctuations and hydrodynamic self-diffusion of sedimenting non-brownian spheres, *Physics of Fluids* **7**, 12 (1995).
- [4] J.-Z. Xue, E. Herbolzheimer, M. Rutgers, W. Russel, and P. Chaikin, Diffusion, dispersion, and settling of hard spheres, *Physical review letters* **69**, 1715 (1992).
- [5] P. J. Mucha, S.-Y. Tee, D. A. Weitz, B. I. Shraiman, and M. P. Brenner, A model for velocity fluctuations in sedimentation, *Journal of fluid mechanics* **501**, 71 (2004).
- [6] R. H. Davis and A. Acrivos, Sedimentation of noncolloidal particles at low reynolds numbers, *Annual Review of Fluid Mechanics* **17**, 91 (1985).
- [7] S. Ramaswamy, Issues in the statistical mechanics of steady sedimentation, *Advances in Physics* **50**, 297 (2001).
- [8] T. Brzinski III and D. Durian, Observation of two branches in the hindered settling function at low reynolds number, *Physical Review Fluids* **3**, 124303 (2018).
- [9] J. Richardson and W. Zaki, Sedimentation and fluidisation: Part i, *Chemical Engineering Research and Design* **75**, S82 (1997).
- [10] G. Batchelor, Sedimentation in a dilute dispersion of spheres, *Journal of fluid mechanics* **52**, 245 (1972).
- [11] G. Taylor, Motion of axisymmetric bodies in viscous fluids, *Problems of hydrodynamics and continuum mechanics* **718** (1969).
- [12] G. Batchelor, Slender-body theory for particles of arbitrary cross-section in stokes flow, *Journal of Fluid Mechanics* **44**, 419 (1970).
- [13] M. B. Mackaplow, *A study of the transport properties and*

- sedimentation characteristics of fiber suspensions* (Stanford University, 1996).
- [14] M. B. Mackaplow and E. S. Shaqfeh, A numerical study of the sedimentation of fibre suspensions, *Journal of Fluid Mechanics* **376**, 149 (1998).
- [15] J. Happel and H. Brenner, *Low Reynolds number hydrodynamics: with special applications to particulate media*, Vol. 1 (Springer Science & Business Media, 2012).
- [16] J. Happel and R. Pfeffer, The motion of two spheres following each other in a viscous fluid, *AIChE Journal* **6**, 129 (1960).
- [17] R. Chajwa, N. Menon, and S. Ramaswamy, Kepler orbits in pairs of disks settling in a viscous fluid, *Physical Review Letters* **122**, 224501 (2019).
- [18] S. Jung, S. Spagnolie, K. Parikh, M. Shelley, and A.-K. Tornberg, Periodic sedimentation in a stokesian fluid, *Physical Review E* **74**, 035302 (2006).
- [19] R. Chajwa, N. Menon, S. Ramaswamy, and R. Govindarajan, Waves, algebraic growth, and clumping in sedimenting disk arrays, *Physical Review X* **10**, 041016 (2020).
- [20] J. M. Crowley, Viscosity-induced instability of a one-dimensional lattice of falling spheres, *Journal of Fluid Mechanics* **45**, 151 (1971).
- [21] B. Herzhaft, É. Guazzelli, M. B. Mackaplow, and E. S. Shaqfeh, Experimental investigation of the sedimentation of a dilute fiber suspension, *Physical review letters* **77**, 290 (1996).
- [22] B. Herzhaft and É. Guazzelli, Experimental study of the sedimentation of dilute and semi-dilute suspensions of fibres, *Journal of Fluid Mechanics* **384**, 133 (1999).
- [23] É. Guazzelli and J. Hinch, Fluctuations and instability in sedimentation, *Annual review of fluid mechanics* **43**, 97 (2011).
- [24] B. Metzger, E. Guazzelli, and J. E. Butler, Large-scale streamers in the sedimentation of a dilute fiber suspension, *Physical review letters* **95**, 164506 (2005).
- [25] B. Metzger, J. E. Butler, and É. Guazzelli, Experimental investigation of the instability of a sedimenting suspension of fibres, *Journal of Fluid Mechanics* **575**, 307 (2007).
- [26] G. H. Golub, Some modified matrix eigenvalue problems, *SIAM review* **15**, 318 (1973).
- [27] G. H. Golub and C. F. Van Loan, An analysis of the total least squares problem, *SIAM journal on numerical analysis* **17**, 883 (1980).
- [28] M. A. Turney, M. K. Cheung, R. L. Powell, and M. J. McCarthy, Hindered settling of rod-like particles measured with magnetic resonance imaging, *AIChE Journal* **41**, 251 (1995).
- [29] See Supplemental Material at URL-will-be-inserted-by-publisher for more details of data, methods and analysis.
- [30] P. Hertz, Über den gegenseitigen durchschnittlichen abstand von punkten, die mit bekannter mittlerer dichte im raume angeordnet sind, *Mathematische Annalen* **67**, 387 (1909).
- [31] S. Chandrasekhar, Stochastic problems in physics and astronomy, *Reviews of modern physics* **15**, 1 (1943).